Journal of Statistical Physics, Vol. 23, No. 3, 1980

Trajectory Divergence for Coupled Relaxation Oscillators: Measurements and Models

J. P. Gollub,[1] E. J. Romer,[1] and J. E. Socolar[1]

Received December 28, 1979

The exponential divergence of nearby phase space trajectories is a hallmark of nonperiodic (chaotic) behavior in dynamical systems. We present the first laboratory of measurements of divergence rates (or characteristic exponents), using a system of coupled tunnel diode relaxation oscillators. This property of sensitive dependence on initial conditions is reliably associated with broadband spectra, and both methods are used to characterize the motion as a function of the coupling strength and natural frequency ratio of the two oscillators. A simple piecewise linear model correctly predicts the major periodic and nonperiodic regions of the parameter space, thus confirming that the chaotic behavior involves only a few degrees of freedom.

KEY WORDS: Dynamical systems; oscillators; chaos; turbulence; nonlinear phenomena.

1. INTRODUCTION

Nonperiodic motion is dissipative dynamical systems is extremely sensitive to initial conditions. Two trajectories in phase space that initially differ by a small amount will separate exponentially in time, and the rate of divergence, averaged along a trajectory, is one way of characterizing the degree of nonperiodicity or irregularity of the motion.[1,2] The divergence rate has been computed in numerical studies,[3–7] but has not been previously measured in laboratory studies of nonperiodic motion. We have investigated an electronic system of coupled tunnel diode oscillators[8] that exhibits nonperiodic behavior in some regions of its parameter space and periodic behavior in others. We find that positive divergence rate is reliably associated with continuous (broadband) spectra, a more conventional diagnostic criterion for nonperiodicity in experiments.

Work supported by the National Science Foundation and the Research Corporation.

[1] Physics Department, Haverford College, Haverford, Pennsylvania.

0022-4715/80/0900-321$03.00/0

We have also performed numerical computations on a simple model for this electronic system, using both spectra and divergence rate to characterize the motion as a function of the coupling strength and natural frequency ratio of the two oscillators. The model generally reproduces the behavior of the laboratory system. In particular, it exhibits nonperiodic motion for appropriate choices of parameters. By comparing the circuit with the model, we have been able to confirm that the nonperiodic time dependence is intrinsic and of macroscopic origin. The demonstration of fairly detailed agreement between a physical nonperiodic system and a corresponding model is perhaps useful in view of the general difficulty of comparing experiments and models of the onset of turbulence.[9–13]

2. COUPLED TUNNEL DIODE OSCILLATORS

The oscillator system used in this study is shown in Fig. 1a. It consists of two coupled relaxation oscillators based on tunnel diodes, each of which has the current–voltage characteristic shown in Fig. 1b. To understand the functioning of this circuit, consider a single oscillator (the left-hand loop of Fig. 1a, for example) in isolation. For an appropriate choice of the driving voltage V_0 and resistance R_1, an instability drives the circuit into oscillations in which the loop shown in Fig. 1b is repetitively executed in a time of the order of L_1/R_1. The current I_{D1} then has the form of rising and descending exponentials, and the voltage V_{D1} switches between roughly constant high and low values when I_{D1} attains threshold values I_α or I_β.

The system actually studied consists of two of these oscillators coupled together by the conductance $G_c \equiv 1/R_c$ (Fig. 1a). Its state is described by a point in a four-dimensional phase (or state) space with coordinates V_{D1}, V_{D2}, I_{D1}, and I_{D2}. The coupling causes the current through each diode to

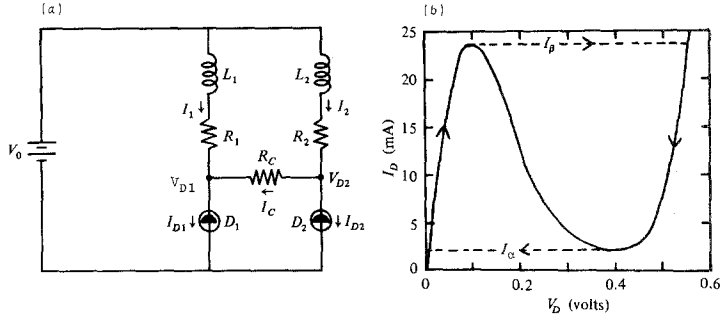

Fig. 1. (a) Tunnel diode oscillator circuit. Each oscillator consists of an inductor, a resistor, and a tunnel diode; the two oscillators are coupled by the resistor $R_c = 1/G_c$. (b) Current–voltage characteristic of the tunnel diode (in series with a 1-Ω shunt resistor). The switching currents are I_α and I_β. Arrows indicate the path of oscillation.

depend on the voltage difference $V_{D2} - V_{D1}$, and can result in induced switching of one oscillator by the other.

We have previously shown[8] that this system exhibits nonperiodicity for certain values of V_0, as indicated by power spectra of V_{D1} and V_{D2}. A theoretical discussion of a somewhat different tunnel diode system has been given by Rabinovich.[13] In this paper we show experimentally (Section 4) that the circuit also has the expected property of exponential divergence of trajectories in phase space when the spectra indicate nonperiodicity, and we map out the regions of nonperiodicity in the space defined by two parameters: the coupling conductance G_c, and the frequency ratio of the uncoupled oscillators $F_0 \equiv (f_1/f_2)_0$. We then show in Section 6 that most of the observations can be obtained from a simple model.

3. DETECTION OF NONPERIODICITY

Reliable criteria for detecting nonperiodicity in laboratory experiments are important. It is not sufficient simply to note erratic time dependence, since such behavior may actually be quasiperiodic, a superposition of discrete frequencies.[9] A common method is to identify nonperiodic motion by a continuous (broadband) spectrum. This criterion can in principle also be misleading, because of the finite spectral resolution in any laboratory or numerical experiment. Another approach sometimes used in numerical computations is to calculate the sensitivity of the system to perturbations. Periodic motion is typically insensitive to small perturbations. For nonperiodic motion, trajectories which are initially separated by a small amount will diverge from each other exponentially, on the average. Here we show that the divergence rate can sometimes be measured in laboratory experiments, even though initial conditions cannot be controlled.

The divergence rate is defined[1] by the expression

$$h(x_0) = \lim_{\tau \to 0} \{(1/\tau) \lim_{d \to 0} \ln[d(\tau)/d]\} \tag{1}$$

where $d(\tau)$ is the separation of a selected trajectory from another at a time interval τ after their separation was d, and the bar indicates an average over the selected trajectory (beginning at x_0) while keeping d constant. The quantity $h(x_0)$ gives the rate of exponential divergence, averaged over a trajectory that begins at x_0. It is generally expected to be a constant for all initial conditions leading to a given nonperiodic attracting set, so we will omit the argument x_0. (It is also equal to the maximum Lyapunov characteristic exponent for the growth of small displacements in the various coordinate directions,[3] and is closely related to the Kolmogorov–Sinai dynamical entropy[14] which frequently appears in the literature on ergodic theory.)

In laboratory experiments, it is useful if possible to work with discrete time systems rather than flows, by observing only the repetitive intersections of trajectories with a fixed hyperplane in phase space on which one or more variables are constant. The corresponding mapping of the hyperplane onto itself is generally called a return map or Poincaré map,[15] and may be specified by a transfer function $x_{i+1} = f(x_i)$. The divergence rate is then

$$h = \lim_{N\to\infty} \lim_{d\to 0} \frac{1}{N} \sum_{n=1}^{N} \ln \frac{d_n}{d} \tag{2}$$

where d_n is the distance between the images of two points separated by d prior to application of the mapping. In this expression, the sum over n plays the role of the time average in Eq. (1). In the simplest case of a one-dimensional map, where the domain of $f(x)$ is a line, Eq. (2) has a simple geometrical interpretation. It can be rewritten[7] as

$$h = \lim_{N\to\infty} \frac{1}{N} \sum_{n=1}^{N} \ln|f'(x_n)| \tag{3}$$

where $|f'(x_n)|$ is the magnitude of the slope of the transfer function at x_n. Thus h is just the average logarithm of the magnitudes of the slopes at points visited by iteration of the map. The shape of the return map can therefore be used to determine the divergence rate, a positive value being indicative of nonperiodic motion.

4. LABORATORY EXPERIMENTS: POINCARÉ MAPS, DIVERGENCE RATES, AND SPECTRA

The circuit shown in Fig. 1 was constructed with attention to the minimization of stray inductance, capacitance, and external noise. The diodes were 1N3720, and the inductors were copper coils with a few ohms resistance wound on ferrite cores. One inductor was fixed at 7 mH, while the other could be varied by withdrawing a ferrite core which was attached to a micrometer. This allowed the frequency ratio F_0 of the uncoupled oscillators to be varied continuously and reproducibly to a precision of 0.5%. The coupling conductance G_c was noninductive and could also be varied smoothly over a wide range. The constant-voltage source was provided by a regulated dc power supply with stability of 0.1% and inductance less than 2×10^{-3} mH. The circuit was well shielded, and 1-kΩ resistors in series with the output terminals reduced the possibility that noise from external sources could create significant currents in this low-impedance circuit. The diode currents were monitored using 1-Ω shunt resistors (not shown) in series with the diodes. The voltages V_{D1} and V_{D2} thus included a small contribution (about 3% of the maximum voltage) from these shunt resistors.

Return maps were constructed with the aid of sample-and-hold devices and a laboratory computer, as shown schematically in Fig. 2. Our object was to obtain a one-dimensional mapping of the form $(I_{D2})_{n+1} = f((I_{D2})_n)$ and this was achieved as follows. The sampling process was initiated each time V_{D1} passed through the value 0.42 V in the decreasing sense. The current–voltage characteristic then constrained I_{D1} to be 5 mA. A negative going step from the comparator triggered the sample-and-hold circuits and enabled the analog-to-digital converter after a 15-μs aquisition time had elapsed. In this way, I_{D2} and V_{D2} were measured essentially instantaneously in comparison with the characteristic time scale of the circuit. (The natural frequencies were about 1000 Hz.) Typically, we sampled I_{D2} and V_{D2} 1000 times to construct a return map. The final step was to sort the data to include only points for which $V_{D2} < 0.2$ V. This restricted I_{D2} and V_{D2} to the left-hand segment of the characteristic in Fig. 1b, where there is a one-to-one functional relationship between them. Thus, I_{D2} determined V_{D2}, and hence the *next* value of I_{D2} as well (since V_{D1} and I_{D1} were fixed). By this sampling process, a one-dimensional mapping was obtained.

Two examples of the resulting maps are shown in Fig. 3. The first one was made in a phase-locked periodic state in which the ratio of the mean frequencies is $F \equiv \bar{f}_1/\bar{f}_2 = 15/8$. As expected, the return map consists of only a discrete set of points, except for an initial transient, which is not shown. The divergence rate for this periodic state is negative, as can be verified by examining the transient behavior. By changing G_c and F_0, qualitatively different return maps are obtained which consist of a small number of smooth lines with discontinuities between them, as shown in Fig. 3b. In this particular case, there are three lines with slopes of magnitude 0.24, 0.95, and 2.15. Taking logarithms and weighting these values by their frequency of occurrence, we find $h = 0.40 \pm 0.05$. Thus, the divergence rate, averaged along the

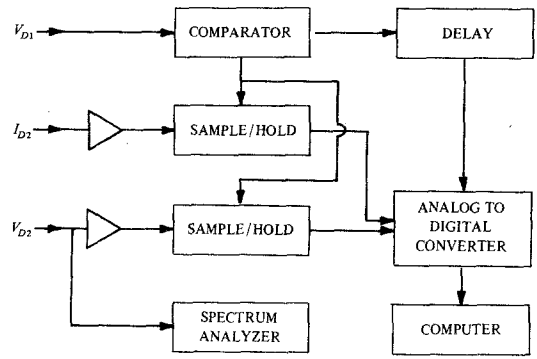

Fig. 2. Block diagram showing the experimental method for obtaining return maps. I_{D2} and V_{D2} are measured when V_{D1} passes through the value 0.42 V in the decreasing sense.

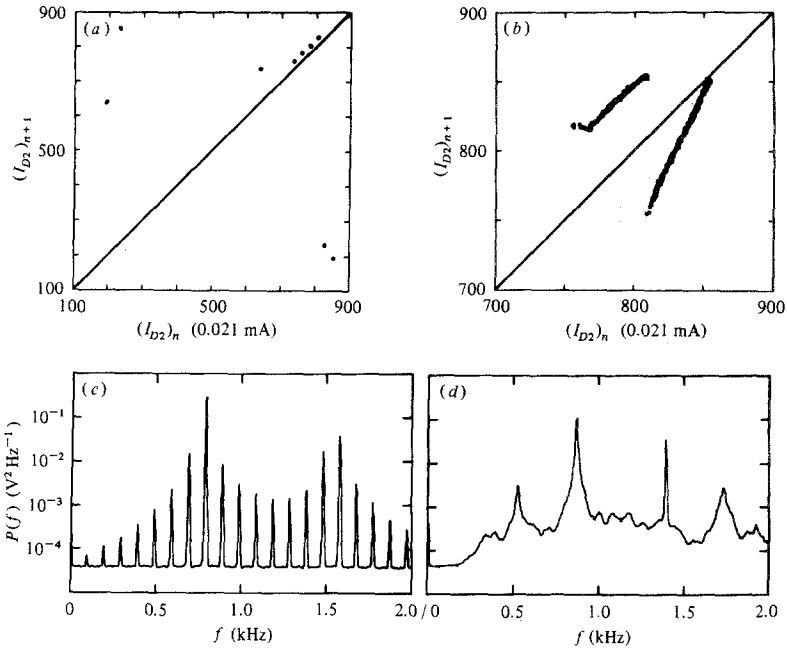

Fig. 3. Return maps and spectra for the actual circuit. (a) Return map of a phase-locked periodic state for which $F \equiv \bar{f}_1/\bar{f}_2 = 15/8$ ($G_c = 0.0055\,\Omega^{-1}$ and $F_0 = 1.911$). The unit of current corresponds to the least significant bit of analog-to-digital conversion. (b) Return map for a nonperiodic state with positive divergence rate ($G_c = 0.0085\,\Omega^{-1}$, $F_0 = 1.798$, and $F = 1.604$). (c) Power spectrum of V_{D2} corresponding to (a). The peaks are instrumentally sharp. (d) Power spectrum of V_{D2} corresponding to (b). Broadband noise is present and the peaks have measurable width.

trajectory, is positive; the motion is therefore nonperiodic for this particular choice of parameters (and perhaps initial conditions).

Power spectra of V_{D2} were obtained with a 400-channel real-time spectrum analyzer, and two examples are shown in Figs. 3c and 3d. The first one corresponds to the periodic state of Fig. 3a, and is composed of instrumentally sharp peaks. The largest is at the mean frequency $\bar{f}_1$ of this oscillator, and the others are at multiples of $\bar{f}_1/8$, which is the inverse of the period of the coupled oscillator system. The baseline noise level is instrumental noise in the measuring system, and does not represent noise in the tunnel diode circuit. It is many orders of magnitude weaker than the spectral peaks associated with the oscillations. A spectrum of V_{D2} for the state with positive h is shown in Fig. 3d. Here there is a substantial amount of broadband noise. Although the peaks still appear to be fairly sharp, examination at much higher resolution indicates that their linewidth is finite. Thus, the spectrum is broadband to within the experimental resolution. We examined

many states and found that positive h is reliably associated with broadband noise. The combination of these two properties is fairly conclusive evidence for nonperiodicity.

We explored the G_c–F_0 parameter space (see Section 2) by varying F_0 for 25 values of G_c, taking spectra continuously and return maps at selected points in order to delineate the periodic and nonperiodic regions. Other parameters were held fixed: $V_0 = 0.260$ V, $R_1 = 4.3\,\Omega$, $R_2 = 4.4\,\Omega$, and $I_2 = 7$ mH. The results are summarized in Fig. 4a. Some regions of the parameter space are periodic and phase-locked at small integer ratios, and are labeled by the ratio F of the mean frequencies of the two oscillators. (This was easily measured by electronic counting.) Other regions labeled N are predominantly nonperiodic, although there are some isolated periodic

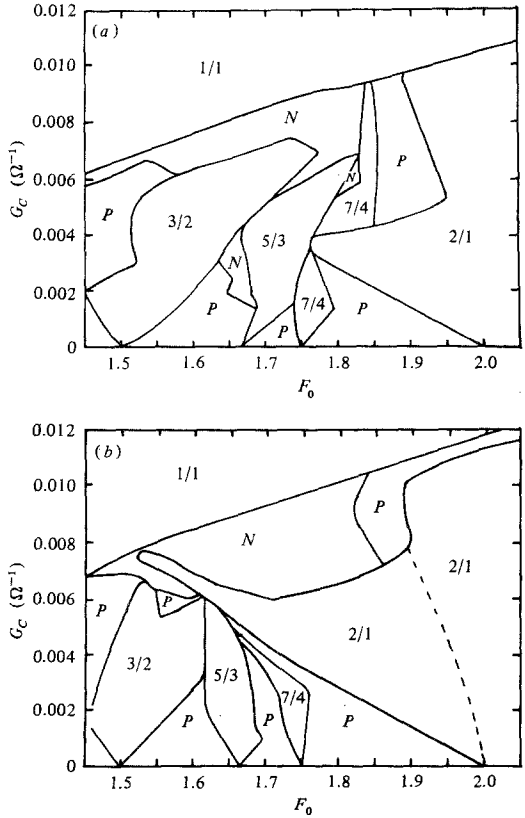

Fig. 4. Parameter space defined by the coupling conductance G_c and uncoupled frequency ratio F_0. Some of the larger periodic regions are labeled by the frequency ratio $F \equiv \bar{f}_1/\bar{f}_2$, while those with higher integer ratios are simply denoted P. Nonperiodic regions are denoted N. The region to the left of the dashed line is phase-locked with short-term fluctuations.

points within them. Regions labeled P are clearly periodic and phase-locked, but F takes on many different values within these regions. For sufficiently strong coupling, $F = 1.00$ regardless of the uncoupled frequency ratio F_0. As the coupling is decreased to zero, F approaches F_0 and the behavior becomes quasiperiodic.

5. A SIMPLE NUMERICAL MODEL

It is possible in principle that the nonperiodic time evolution of this system of coupled relaxation oscillators is caused by microscopic processes or external noise. In order to exclude these possibilities, and to better understand the origin of the nonperiodicity, we constructed a simple model whose behavior could be accurately computed. The circuit obeys the following equations if stray inductance and diode capacitance are neglected:

$$L_1\, dI_1/dt = V_0 - I_1R_1 - V_{D1}, \qquad L_2\, dI_2/dt = V_0 - I_2R_2 - V_{D2}$$
$$I_c = G_c(V_{D2} - V_{D1}), \qquad I_{D1} = I_1 + I_c, \qquad I_{D2} = I_2 - I_c \tag{4}$$

We approximated the current–voltage characteristic of the diode to be rectangular, so that $V_{D1} = V_L$ (a constant) as the current increases from I_α to I_β, and $V_{D1} = V_H$ (a constant) as the current decreases from I_β back to I_α. However, we included in V_L and V_H the voltage drop across the diode caused by the coupling current I_c:

$$V_L = |I_cR_D|, \qquad V_H = 0.45V - |I_cR_D| \tag{5}$$

where the diode resistance R_D was taken to be 5 Ω.

The advantage of these approximations is that the diode voltages change only in discrete steps, and the equations are linear in the intervals between these discontinuities. Therefore they can be solved exactly to yield $I_{D1}(t)$ and $I_{D2}(t)$ in these intervals for given initial conditions. For example, if both diodes are in the low-voltage state, the current I_{D1} is of the form

$$I_{D1}(t) = Ae^{\gamma t} + C \tag{6}$$

and it will switch when $I_D(t) = I_\beta$. This occurs at a time

$$t = \frac{1}{\gamma} \ln \frac{I_\beta - C}{A} \tag{7}$$

provided the other diode does not switch sooner.

In this fashion, the behavior of the model can be computed accurately over 1000 or more oscillations without the errors that often build up when integrating differential equations over such long times. Computations were done in double precision (17 significant figures) on a PDP 11/10, and the

currents are estimated to be accurate to about one part in 10^7 over 1000 oscillations.

We obtained return maps by computing I_{D1} each time $V_{D1} = V_L$, $V_{D2} = V_H$, and $I_{D2} = I_\beta$, so that D_2 had just switched. Sequential values of I_{D1} were then plotted as $(I_{D1})_{n+1}$ versus $(I_{D1})_n$, as for the experiments on the actual circuit. The divergence rate was obtained using Eq. (2), except that the limits were replaced by $d = 0.01$ mA and a value of n in the range $300 < n < 2000$.

In order to compare different methods of identifying nonperiodicity, and to facilitate comparison with the experiments, we computed spectra of the diode voltages for the numerical model. Each voltage is composed of a series of irregularly spaced square pulses $A_k(t)$ of height $V = V_L$ or V_H for the interval $t_{1k} < t < t_{2k}$. The Fourier transform of $A_k(t)$ is just

$$A_k(\omega) = \frac{V}{i\omega(2\pi)^{1/2}} [\exp(i\omega t_{2k}) - \exp(i\omega t_{1k})] \tag{8}$$

The desired power spectrum of the entire pulse train is then the magnitude squared of $A(\omega) = \sum_k A_k(\omega)$. However, the finite length of the pulse train broadens the trails of spectral peaks. To mitigate this effect, we use a windowing technique (the "GEO window"[16]) in which $A(\omega)$ is convolved with a windowing function before squaring.

Before describing the results of these computations, we note that there is a large literature on the mathematics and numerical simulation of nonlinear oscillators. Chirikov[17] has recently reviewed this subject, with emphasis on Hamiltonian systems rather than the dissipative system considered here. Our main purpose in studying the behavior of this model is to better understand the experimental observations discussed earlier.

6. NUMERICAL RESULTS AND COMPARISON

We computed return maps, divergence rates, and (sometimes) spectra for several hundred points in the parameter space defined by G_c and F_0 while keeping other parameters constant: $V_0 = 0.17$ V, $R_1 = 4.3\,\Omega$, $R_2 = 4.2\,\Omega$, $I_\alpha = 3$ mA, $I_\beta = 22$ mA. Examples of return maps and spectra are shown in Fig. 5. The first return map corresponds to a periodic state with the oscillators locked at the ratio $F = 15/8$. After an initial transient, the mapping converges to the set of eight points shown on the graph. The divergence rate is clearly negative: $h = -0.134$. Other regions of the parameter space yield nonperiodic time dependence, as shown, for example, by the return map of Fig. 5b, which is composed of steep lines rather than discrete points. In this case, $h = 0.684 \pm 0.005$. The dependence of h on F_0 at constant $G_c = 0.008\,\Omega^{-1}$

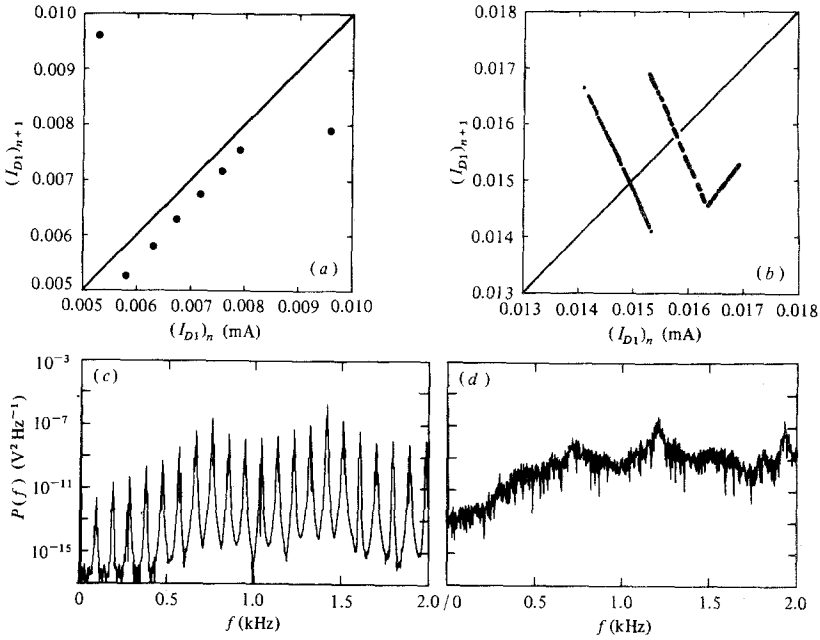

Fig. 5. Return maps and spectra for the numerical model. (a) Return map of a phase-locked periodic state for which $F = 15/8$ ($G_c = 0.0090\,\Omega^{-1}$ and $F_0 = 1.880$). (b) Return map for a nonperiodic state with positive divergence rate ($G_c = 0.0075\,\Omega^{-1}$ and $F_0 = 1.689$). (c) Power spectrum of V_{D1} corresponding to (a). The peaks are instrumentally sharp. (d) Power spectrum of V_{D1} corresponding to (b), showing the presence of broadband noise.

(Fig. 6) demonstrates that the distinction between the periodic and nonperiodic regions is clearly evident from the sign changes of h.

A numerically computed spectrum corresponding to Fig. 5a is shown in Fig. 5c, and it has the features generally expected of a periodic system. The peaks are as sharp as the numerical resolution (0.0025 kHz), although the logarithmic scale makes them appear wider. In addition, the largest peaks are at least eight orders of magnitude above the background noise level (at the lower left side of the graph), which is presumed to be numerical noise generated by the finite computational accuracy. This spectrum has dynamic range and resolution superior to what is normally attainable in experiments. It nevertheless bears a remarkable resemblance to that obtained from the actual tunnel diode circuit (Fig. 3a), except that the largest peak is the 15th one instead of the 8th one. This difference is caused solely by the fact that the numerical spectrum was computed for the faster oscillator (V_{D1}), while the experimental spectrum was measured for the slower one (V_{D2}). A spectrum corresponding to the nonperiodic state of Fig. 5b is shown in Fig. 5d. It consists predominantly of broadband noise, as one might expect

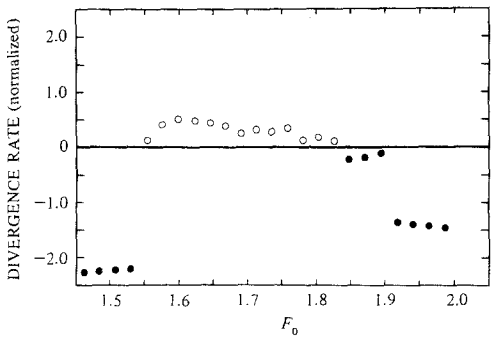

Fig. 6. Dependence of the divergence rate on uncoupled frequency ratio F_0 for the model, showing that the regions of positive h (open circles) are easily recognized.

from the large divergence rate. For the model, as for the circuit, broadband spectra and positive divergence rate occur together. For states which had a very low level of noise ($h < 10^{-3}$) positive divergence rate seemed to be a more sensitive indicator of nonperiodicity than broadband spectra. In these cases the spectra were ambiguous, consisting of many overlapping peaks.

The G_c–F_0 parameter space is shown in Fig. 4b. Although it was computed for a value of V_0 different from that of Fig. 4a, the resemblance between the experimental and computed behavior is striking. Both the circuit and the model show a large phase-locked and periodic 1/1 region at the upper left, and other phased-locked regions at the same locations, and of about the same extent. In particular, the 3/2 and 5/3 regions are similar in the two cases, and the line separating the 2/1 state from the more complex periodic states below it has almost exactly the same slope in the two cases. Most importantly, both the circuit and the model show a large region of nonperiodic behavior near the center of the diagram.

There are also several apparent differences between the experimental and computed parameter space diagrams. The circuit shows several smaller nonperiodic regions that are missing from the model. Furthermore, the 2/1 region of the model shows a large protrusion (to the left of the dashed line) in which the divergence rates are clearly positive, while the spectra consist of fairly sharp peaks coexisiting with noise.[2] These states are phase-locked only on the average, with nonperiodic short-term fluctuations. Such phase-locked nonperiodic states have not been detected in the circuit. However, it is possible that this difference is an artifact of the particular diagnostic techniques that were employed, which are more sensitive to nonperiodicity in the model than in the circuit. For example, the 10-bit accuracy of the analog-to-digital conversion does not permit the sign of h to be determined if $|h| < 0.05$ or if the

[2] This phenomenon has recently been called "semiperiodicity" by E. N. Lorenz (preprint).

lines of the return map are very short. On the other hand, it is also possible that this difference between the model and the laboratory system is due to the rectangular approximation to the I–V characteristic of the diodes.

It should be noted that Figs. 4a and 4b are sections of a parameter space of higher dimensionality. The structure of this space depends somewhat on the parameters held constant, and this may cause some of the differences between the two figures. Brief scans of this plane at other voltages indicated that the shapes of the regions more closely approximate those of Fig. 4a for some other values of V_0. We chose 0.17 V for a detailed scan because it yielded high values of h. (We did not expect the numerical value of V_0 to match that of the circuit, because of the approximations we made for the diode characteristics.)

Caution is also necessary in discussing the relationship between Fig. 4a and Fig. 4b because of the possible effects of hysteresis, and the dependence on initial conditions. In studying the circuit, where initial conditions cannot be freely chosen, we varied the parameters G_c and F_0 monotonically in order to obtain reproducible results. In the model, we simply kept the initial conditions constant. These different ways of dealing with hysteresis could affect the degree of correspondence between the circuit and the model.

7. CONCLUSIONS

Numerical models of dissipative dynamical systems are in widespread use. However, our intent is to test the detailed correspondence between a model and the physical system it represents. That is possible here because there are only a few degrees of freedom, and the circuit equations and diode characteristics are well known. In general we find that the major periodic and nonperiodic regions of the parameter space can be correctly predicted by a simple model. Furthermore, the model yields divergence rates comparable in magnitude to the measured values. The close correspondence between the model's behavior and that of the circuit is convincing evidence that the observed nonperiodicity involves only a few degrees of freedom and is not due to microscopic noise, external noise, or other extraneous effects. This is encouraging, since a similar hypothesis about the origins of fluid turbulence has been much more difficult to establish.

Finally, we have demonstrated that the property of sensitive dependence on initial conditions, or positive divergence rate of phase space trajectories, can be used for the diagnosis of nonperiodic motion in *laboratory* experiments as well as in numerical computations. While this method will not be as straightforward to implement in systems with many degrees of freedom, it does provide a useful alternative to spectral techniques in some cases.

ACKNOWLEDGMENT

We are grateful to R. Landauer for the suggestion that coupled relaxation oscillators might be nonperiodic.

REFERENCES

1. F. M. Zaslavsky and B. V. Chirikov, *Usp. Fiz. Nauk* **14**:549 (1972).
2. D. Ruelle, *Ann. N.Y. Acad. Sci.* **316**:408 (1979).
3. G. Benettin, L. Galgani, and J.-M. Strelcyn, *Phys. Rev. A* **14**:2338 (1976).
4. A. B. Rechester, M. N. Rosenbluth, and R. B. White, *Phys. Rev. Lett.* **42**:1247 (1979).
5. I. Shimada and T. Nagashima, *Prog. Theor. Phys.* **61**:1605 (1979).
6. S. D. Feit, *Commun. Math. Phys.* **61**:249 (1978).
7. N. H. Packard, J. P. Crutchfield, J. D. Farmer, and R. S. Shaw, Geometry from a time series, preprint.
8. J. P. Gollub, T. O. Brunner, and B. G. Danly, *Science* **200**:48 (1978).
9. J. P. Gollub and S. V. Benson, *J. Fluid Mech.*, to appear.
10. A. S. Monin, *Sov. Phys.—Usp.* **21**:429 (1978).
11. G. Ahlers and R. P. Behringer, *Prog. Theor. Phys. Suppl.* **64**:186 (1979).
12. H. L. Swinney and J. P. Gollub, eds., *Hydrodynamic Instabilities and the Transition to Turbulence* (Springer-Verlag, Berlin, New York, 1980).
13. M. I. Rabinovich, *Sov. Phys.—Usp.* **21**:443 (1978).
14. A. S. Wightman, in *Statistical Mechanics at the Turn of the Decade*, E. G. D. Cohen, ed. (Marcel Dekker, New York, 1971), pp. 1–32.
15. R. M. May, *Nature* **261**:459 (1976).
16. R. K. Otnes and L. Enochson, *Digital Time Series Analysis* (Wiley, New York, 1972).
17. B. V. Chirikov, *Phys. Rep.* **52**:265 (1979).